Oxidized Mild Steel S235: An efficient Anode for the Electrocatalytically Initiated Water-Splitting

Dr. Helmut Schäfer[a]*, Dr. Karsten Küpper[b], Prof. Dr. Joachim Wollschläger[b], Dr. Nikolai Kashaev[c] , Dr. Jörg Hardege[d], Prof. Dr. Lorenz Walder[a], Seyyed Mohsen Beladi-Mousavi[a], Brigitte Hartmann-Azanza[a], Prof. Dr. Martin Steinhart[a] , Shamaila Sadaf[a] and Falk Dorn[c]

Abstract: Steel S235 was surface oxidized upon chlorine gas and checked for its electrocatalytic efficiency regarding oxygen formation in aqueous solution. When exposed to humid Cl_2 gas for 110 min steel S235 developed into a electrocatalyst exhibiting an overpotential for the oxygen evolution reaction (OER) of 462 mV at 1 mA/cm^2 at pH 7. The OER activity of the same sample at pH 13 was found to be moderate (347 mV overpotential at 2.0 mA/cm^2 current density) in comparison with recently developed OER electrocatalysts. Potential vs. time plots carried out at constant current demonstrate the sufficient stability of all samples under catalysis conditions at both pH 7 and at pH 13 for tens of hours. High resolution XPS spectra could be reasonably resolved with the proviso that Fe_2O_3, FeO(OH), MnO(OH) and Mn_2O_3 are the predominant Fe respectively Mn- species on the surface of the oxidized steel S235.

[a] Dr. Helmut Schäfer, Prof. Dr. Lorenz Walder, Seyyed Mohsen Beladi-Mousavi, Prof. Martin Steinhart, Brigitte Hartmann-Azanza, Institute of Chemistry of New Materials and Center of Physics and Chemistry of New Materials, Universität Osnabrück, Barbarastrasse 7, 49076 Osnabrück, Germany
E-mail:helmut.schaefer@uos.de

[b] Dr. Karsten Küpper, Prof. Dr. Joachim Wollschläger, Fachbereich Physik, Universität Osnabrück, Barbarastr. 7, 49076 Osnabrück, Germany

[c] Dr. Nikolai Kashaev, Falk Dorn, Institute of Materials Research, Materials Mechanics, Helmholtz-Zentrum Geesthacht, Max-Planck-Str. 1, 21502 Geesthacht, Germany

[d] Dr. Jörg Hardege, School of Biological, Biomedical & Environmental Studies, University of Hull, Cottingham Road, HU6 7RX, Hull, UK

Keywords: *solar to fuel conversion, renewable energy sources, standard Carbon Manganese steel, Surface oxidation, oxygen evolution electrocatalysis, XPS spectroscopy*

Table of Contents

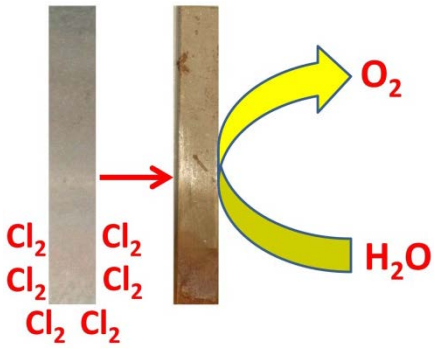

Exposure to chlorine gas at room temperature converts standard carbon manganese steel (S235) into an oxygen evolution electrocatalyst that exhibited a surprising high catalytic activity in neutral regime as shown by the strong voltage current behavior derived from long term chronopotentiometry measurements: 462 mV overpotential at 1 mA/cm^2 in 0.1 M KH_2PO_4/K_2KHPO_4 buffer solution.

Introduction

Solar energy can be captured and stored in the form of chemical bonds in solar fuels (artificial storage of solar energy) [1, 2, 3, 4]. Taking into account the fact that in principle water represents a limitless hydrogen and oxygen source, hydrogen and oxygen production in water electrolyzers is potentially very promising, economical solar to fuel conversion route. In total four electrons have to be transferred within the OER sequence, a requirement that makes the OER complex: $4\ OH^- \rightarrow O_2 + 2\ H_2O + 4\ e^-$. As a consequence large overpotentials are especially caused on the side where OER takes place; therefore it is the anode that usually represents the critical, limiting pole. The anode of an efficient water electrolysis apparatus has to operate as close as possible to Nernstian potentials (E), i.e. the applied potential should not differ strongly from the reversible H_2O/O_2 potential (1.228 V vs. RHE, at standard temperature and pressure) at frequently practiced current densities. A reasonable, often utilised current density of the electrocatalytically driven water-splitting is, due to technical reasons 5-10 mA/cm^2 [5, 6, 7]. Catalysts based on precious metals [8, 9]- or metal oxides fulfill these requirements and especially Rutile type IrO_2 and RuO_2 are considered to be established water-splitting catalysts [10, 11, 12, 13,14, 15, 16, 17] at both, neutral and alkaline regimes. However these metal oxides are costly because of the scarcity of Ir, and Ru, and in addition showed poor stability regarding the long term electrolysis of water especially in alkaline regimes [18]. Research teams led by Strasser and Wark reported on Core-shell architecture based noble metal containing nanoparticles: a possible route not only to reduce the price of noble metal containing catalysts, [19] but also to enhance their stability and efficiency [20]. Nevertheless there is still a lack of efficient, stable and low-priced catalysts made of earth-abundant, affordable elements. Pioneering studies by the groups of J. P. Hoare, A. J. Bard, J. O`M. Bockris and of many other leading scientists performed within the last decades [21, 22, 23] showed that the voltage necessary to produce oxygen on a metal surface is related to the redox potential of the metal/metal oxide couple, or in other words, even in the case of noble metals no oxygen can be released from the surface as long as the corresponding metal oxide is not formed. Although IrO_2 and RuO_2 species were discovered as promising candidates, cheaper catalysts can potentially be found based on the same principle idea. The most important non noble metal based catalytic materials for OER in alkaline medium and in neutral medium shall be reviewed consecutively at this point. MnO_x compounds with different compositions, morphologies and structures have been synthesized using a variety of approaches and studied as a water-splitting catalyst e.g. at pH 13 and 14 [24, 25]. Different Ni-, or Co- or Ni-Co containing oxides like $LaMnO_3$[26], $LaNiO_3$[27], Graphene-Co_3O_4 nanocomposites [28], $NiCo_2O_4$ [22, 29] have been intensively investigated over the past decades and optimized with respect to the water splitting properties. More recently benchmark species such as $Ba_{0.5}Sr_{0.5}Co_{0.8}Fe_{0.2}O_y$ [30], $Pr_{0.5}Ba_{0.5}CoO_y$ [31], $NiCo_2O_4$ –graphene hybrid [32], $NiCo_2O_4$ aerogel [33], Ni_3S_2 nano array supported by Ni metal [34] and $CuFe(MoO_4)_3$ [35] were developed. Besides electrodeposited thin metal containing films, a range of metals and metal alloys including steel have been

investigated and proposed as catalysts for the electrocatalytic OER mainly in alkaline medium. Amongst the most promising candidates is Ni, which has been used commercially and utilized as a catalyst for anodic water splitting [36, 37, 38], NiFe films [39] as first introduced by Corrigan et al. [40, 41], Fe [38, 42, 43], Co[38], Steel [44, 45, 46, 47, 48] and Ni-Co alloys [49, 50]. To the best of our knowledge, the highest activity with steel or iron as a catalyst for the electrochemical assisted splitting of water in alkaline medium was recently achieved by our group [51] with an overpotential of 212 mV at 10 mA/cm^2 in 1 M KOH, by the groups of Lyons and Doyle with 360 mV overpotential at 1 mA/cm^2 in 1 M NaOH [43], respectively 600 mV overpotential at 10 mA/cm^2 in 0.1 M NaOH-, [46] and by Moureaux and Chatenet with 320 mV overpotential at 10 mA/cm^2 in 1 M KOH [45]. Especially the OER properties of pure iron are, at best, moderate (0.55 V vs. RHE at 10 mA/cm^2 in 1 M NaOH) [38].

OER electrocatalysts listed so far require basifying additives. Water-splitting catalysts working under neutral conditions would pave the way for a virtually direct utilization of seawater as a potential source for H_2 + O_2, usable for example as fuel suitable for the fuel cell. Inspired up to some extent by nature, the OER occurs in photosystem II (PS II), which is present in green plants, algae, and cyanobacteria [52], recent efforts over the past 5-7 years focused on OER and hydrogen evolution reaction (HER) performed at values close to neutral pH 7 [6, 53, 54]. In general, overpotentials required to guarantee a reliable current density for the OER are significantly higher when the electrochemical cleavage of water is performed under neutral conditions. Thus even when electrodes were found to be highly attractive anodes for water-splitting at pH values between 13 and 14, is by no means guaranteed, that they show also in neutral regime superior OER charactersitics. Sandwich structured layer systems consisting of gold oxide and iron-oxide and [55] single layers consisting of iron oxide such as FeO(OH) have been achieved via anodic deposition and checked for its water-splitting properties at pH 7.2 more than 30 years ago [56, 57].

At large, the obtained overpotential for OER on recently developed materials at pH values between 4 and roughly 7 are relatively close to 500 mV at 1 mA/cm^2 current density in 0.1 M K_2HPO4/KH_2PO_4 [58]. Nanostructured Mn oxides have been found to be active as OER electrocatalysts at pH 5.8 [59] as well as at pH 4 [60]. An overpotential of 610 mV for the onset of OER at pH 6.9 was reported for ZrS_3 nanosheets [61]. Wu et al. reported on 480 mV overpotential achieved at stable current density of 1 mA/cm^2 [58] for iron based thin films. Electrodeposited FeO(OH) [56, 57], cobalt-phosphate compounds [6, 53] and nano-scaled Co-oxides [62] are among the known non noble compounds for which slightly better OER activity (down to 410 mV overpotential at 1 mA/cm^2) has been demonstrated.

Co_3O_4 nanowire arrays [62] developed by He et al. showed an unusual strong voltage-current behavior at pH 7.2. However no steady state measurements performed at pH 7.2 were shown and Faraday efficiency was not determined, which makes it at least difficult to conclusively assess the overpotential for the OER at a predetermined current density. Very recently the OER performance of Graphene-Co_3O_4 nanocomposites have also been investigated under neutral conditions and exhibited very low

overpotentials for the OER derived from cyclic voltammograms (498 mV at 10 mA cm^{-2}). Unfortunately no long term voltage-current behavior was shown and the release of oxygen was not quantified.

Pure metals and metal alloys have very rarely been proposed as OER electrocatalysts in neutral regimes [48] and the few studies carried out showed that the superior OER properties of Ni containing steel is at least up to some extent restricted to water-splitting in alkaline media [48]. Mild steel, e.g. steel S235 (standard Carbon Manganese steel) is based on promising ingredients manganese and iron, and as such represents an interesting candidate for the reduction of the overpotential caused at the anode during OER in alkaline and neutral media, and that has to the best of our knowledge, not been exploited so far for this purpose. Iron for instance is the most abundant transition metal in the earth`s crust, and is less toxic than Co and Ni. Steel S235 is much cheaper than pure iron available from laboratory chemicals suppliers as well as stainless steel. The suitability of steel S235 a cheap, non-toxic, and commonly available material as an OER electrode at pH 7 and at pH 13 was evaluated within this study. Supplementary we checked whether an enhancement of the electrocatalytic oxygen evolution characteristics upon chlorination of the surface at room temperature can be realized.

Chlorination and ozonation of steel is an established technique for the disinfection of surfaces [63] but also for use in the recycling of steel and healing processes of steel surfaces [64]. To the best of our knowledge Cl_2 gas has rarely been used for the surface oxidation of steel in order to improve the electrocatalytic properties with respect to OER [48].

Sample list

Sample	1	2	3	4	Ref	IrO_2-RuO2
Treatment	Cl_2	Cl_2	Cl_2	Cl_2	-	-
Temperature [K]	293	293	293	293	293	293
Duration [min]	110	190	500	720	-	-
Overpot. [mV] at pH 13	347	362	382	390	462	-
Overpot. [mV] at pH 7 7	462	512	598	602	-	-
Figure	1a,1c, 4b, S2	4c, 6e, S2	S2, S6a, S6b	4d, 6f, S2, S8	1d, 4a, 6a, S2	1c

Table 1 Overview of the prepared samples/ surface oxidation procedures. Images of the surface oxidized steel samples1-4 can be taken from Figure S3. An apparent surface area of ~ 1.5 cm^2 was defined by an insulating tape (Kapton tape). The overpotential was determined in 0.1 M KOH (pH 13) at 2 mA/cm^2 respectively in 0.1 M KH_2PO_4/ K_2HPO_4 at 1 mA/cm^2 (pH 7).

1 Results and discussion

Table 1, Figure S3 gives an overview of the samples respectively the electrochemical key data and the basic synthesis parameter of all samples discussed in this contribution.

1.1 Properties of chlorinated steel S235 in alkaline regime

1.1.1 The OER characteristics

Within the chlorine treated test series, sample 1, stainless steel which was exposed to Cl_2 for 110 min showed the best catalytic performance (Table 1, Figure 1, 3, 4) in neutral and alkaline regimes and therefore creates the basis for the overarching discussion of the electrochemical- and kinetic properties of the samples and the mechanistic investigations of the OER presented in sections 1.1 and 1.2 of this contribution. An impression of the electrochemical steady state performance of sample 1 at pH 13 can be derived from Figure 1a-d. Long term chronopotentiometry measurements performed in 0.1 M KOH exhibited an relatively strong voltage-current behavior: 1.575 V *versus* RHE for 2 mA/cm^2 current density which would correspond to 347 mV overpotential for the OER. In addition a very good stability of the potential required for 2 mA/cm^2 current density even after tens of hours operating time was obtained (Figure 1a). The increase of the potential required to guarantee 3 mA total current (2 mA/cm^2 current density) was determined to be 30 mV within 100000 s (Figure 1a). At 10 mA/cm^2 current density the required potential amounted to 1.644 V versus RHE which corresponds to 416 mV overpotential for the OER (Figure S4). The oxide layer obviously establishes a stable periphery, which therefore stabilizes the sample outwardly: Sample 1 showed no weight loss even after longer operating times (100000 s chronopotentiometry at 2 mA/cm^2 in 0.1 M KOH, Table S2) and an analysis of the electrolyte after long time experiments did not reveal Fe ions (See supporting information's). Both findings suggest that the current measured during the chronopotentiometry very likely does not arise from oxidation or dissolution. However to further exclude an oxidation of the metal matrix below the oxide layer ("inner oxidation") during operating which would inevitably falsify the OER performance it is indispensable to quantify the real oxygen evolution efficiency. We determined the Faradaic efficiency of sample 1 (Figure 1b, top panel) during 3000 s of chronoptentiometry (Figure 1b, lower panel). The experiment was performed as described in the supporting information. The curve course of the dissolved oxygen in 0.1 M KOH during chronopotentiometry conducted at 2 mA/cm^2 with the time (black curve) shows a good agreement with the theoretically possible increase of dissolved oxygen on the basis of 100% charge to oxygen conversion (100% Faradaic efficiency; red line). The Faradaic efficiency of the OER of sample 1 in 0.1 M KOH at 2 mA/cm^2 and at ~360 mV overpotential for the OER was found to be 67% after 3000 s running time proving the overall acceptable electrocatalytic oxygen evolution properties (Table S3). Low Faradaic efficiencies at relatively high current densities do not necessarily indicate an oxidation/dissolution of the catalysts itself, but can up to some extent, be caused by

measurement inaccuracies. During the measurement gas bubbles visible by the eye were released from the sample surface. We assume that at the applied potential apparently undissolved oxygen gas bubbles are generated, i.e. oxygen cannot be dissolved with the speed with which it is formed. A significantly decreasing Faradaic efficiency by increasing current densities (From 97% at 1 mA/cm^2 to 43% at 10 mA/cm^2) was obtained by Qiu et al. (2014) for Ni-Fe containing nanoparticles in 1 M KOH [65]. In terms of the electrocatalytic activity of sample 1 we obtained a reinforced electro catalytic performance, compared with pure iron and some iron alloys [49, 50, 66]. Lyons and Doyle reported on the activation of iron via cyclic oxidation in alkaline medium and found for the overpotential in 0.1 M NaOH values around 600 mV at 10 mA/cm^2 [46] respectively 360 mV in 1 M NaOH at 1 mA/cm^2 [43]. However the OER activity of the samples we tested (Figure 1a, Figure S4) in alkaline regimes is substantially below the OER performance of non-activated or activated stainless steel. The highest OER activity determined for 316L steel was reported by Chatenet et al. (330 mV overpotential at 10 mA/cm^2 in 1 M KOH) [45]. We recently reported on the suitability of AISI 304 steel as a potential OER electrocatalyst [48, 51]. Upon Cl_2 activation AISI 304 steel exhibited for the OER in 0.1 M KOH an overpotenttial of 260 mV at 1.5 mA/cm^2[48]. The highest OER activity was achieved when AISI 304 steel was electro-activated for several hours under harsh conditions leading to a Ni enrichment on the surface and finally to a significant reduction of the overpotential down to 212 mV at 12 mA/cm^2 in 1 M KOH [51]. We compared sample 1 with IrO_2-RuO_2, which is considered as an established water splitting catalyst in neutral as well as in alkaline regimes [10, 11]. Differences with respect to the OER currents of both samples at different voltages respectively overpotentials can be extracted from the Tafel plots shown in Figure 1c. As expected, superior electrocatalytic behavior was found for IrO_2-RuO_2 particularly in the lower potential region, but with increasing potential the difference of the potentials required for sample 1 and IrO_2-RuO_2 to initiate a defined OER current decreased. Whereas at 2 mA/cm^2 the difference of these potentials amounted to 120 mV, at 10 mA/cm^2 the voltage-current performance of both samples is separated by only 76 mV and finally almost the same potential is necessary to ensure 16.66 mA/cm^2 current density (sample 1: 1.75 V; IrO_2-RuO_2: 1.72 V). This means that especially in the high potential region IrO_2-RuO_2 loses significantly performance, which is displayed by the rising Tafel slope from 89.8 mV dec^{-1} in lower potential region (Figure 1c) to a value of 186.7 mV dec^{-1} in the higher potential region (Figure 1c). A substantial horizontal shift of the Tafel line assigned to sample 1 compared to the corresponding Tafel line of untreated steel towards lower potentials (Figure 1d) proves the meaningful enhancement of the electrocatalytic properties upon the applied surface oxidation. The gap between both samples concerning the overpotential required for a defined current density increases substantially with increasing current density as can be seen in the corresponding Tafel lines as theses move apart from each other towards higher potential region (Figure 1d). At 2 mA/cm^2 this gap amounted to 42 mV and increased to 60 mV and 100 mV at 4 and 13 mA/cm^2 respectively (Figure 1d). This can in our opinion

only be explained by a change of the chemical nature of the surface of the samples during the surface treatment. Both samples showed Dual Tafel behavior within the investigated potential region with lower slopes at lower overpotential regions (Sample 1: 58.5 mV dec^{-1} ≙ 2.28 x RT/F; Reference: 102 mV dec^{-1}) and higher slopes at higher overpotential regions (Sample 1: 133.7 mV dec^{-1}; Reference: 195.2 mV dec^{-1}). This can be rationally explained by a transition between different OER mechanisms or by different rate determining steps while moving from low to higher overpotential regions. In addition this implies different OER mechanism, different catalytic active species or a different rate determining step on the surfaces of the reference sample and sample 1. Thus the value determined for sample 1 at lower potentials (2.28 x RT/F) agrees well with the value that was found to be characteristic of an O_2 evolution mechanism involving a reversible one-electron transfer (2.3 x RT/F) [67]. Tafel slope values of 45-48 mV dec^{-1} were observed for pure iron electrodes in 1-5 M NaOH solutions [38] whereas earlier papers also reported on slopes of up to 80 mV dec^{-1} in lower potential region in case of fresh Nickel-oxide electrodes [68].

1.1.2 The mechanism of the OER

Varying the KOH concentration between 0.1 and 5 M resulted in the Tafel plot presentated in Figure 2 of sample 1 showing slopes in the range 58.5 mV-66 mV dec^{-1} at lower overpotential regions. For example a slope of 64.7 mV dec^{-1} was determined in 2 M KOH, 58.5 mV dec^{-1} in 0.1 M KOH respectively (Figure 2a). As such it is very likely that there is no significant change either in the OER mechanism or in the rate determining step for sample 1 when we increase from a low (0.1 M) to higher concentrations (0.5, 1, 2 and 5 M).

In this case we would expect a reasonable reaction order when extracted from $(\partial \log i/\partial \log a)_E$ behavior. We checked the $(\partial \log i/\partial \log a)_E$ behavior at constant potential of 1.55 V and 1.59 V *versus* RHE, as such in a potential region at which oxygen formation almost certainly takes place even in case of the lowest chosen KOH concentration (C_{OH^-}= 0.1 mol/l). The slope amounted to 0.462, 0.475 respectively (Figure 2b, 2 c).

Usual single barrier models (interfacial electron transfer) cannot rationalize Tafel slopes significantly higher than 2.303 x 2RT/3F (39.4 mV dec^{-1}at 25 °C) [38]. Approaches based on more complicated systems, such as dual barrier models can help to extract e.g. reasonable reaction orders from $(\partial \log i/\partial \log a)_E$ behavior in cases when the determined Tafel slope differs substantially from 39.4 mV dec^{-1}at 25 °C . Meyer [69] found the following relationship to be valid under dual barrier conditions:

Equation 1

where β_f is the electron transfer symmetry factor for field assisted charge transport through the oxide, β_t is a composite symmetry factor taking account of the two potential energy barriers and m_s is the value of the reaction order based on single barrier condition. Based on a simple assumption that both potential barriers are symmetrical and therefore $\beta_f = \beta_t = 0.5$, m_s amounted to approximately 1 (first order reaction), taken into consideration that $(\partial \log i/\partial \log a)_E = 0{,}462$ at E=1.55 V *versus* RHE, $(\partial \log i/\partial \log a)_E = 0{,}475$ at E=1.59 *versus* RHE respectively (Figure 2b, 2c). This means that the reaction order of ~ 0.5 measured under dual barrier conditions, corresponds to an expected value of $m_s = 1$ in a single barrier treatment of the compatible pathway.

1.1.3 The catalytic active species

Generally X-Ray diffraction is an established appropriate method to characterize oxides formed on steel [70], however XRD experiments performed with our oxidized samples did not lead to significant, straight forward to interpret results. Figure S5 presents the outcome of the XRD experiment performed with sample 4. The diffractogram does not indicate crystalline oxides in the surface layer although the measurements were performed in grazing incidence, i.e. were sensitive to the surface. Most likely the metal oxide layer consists of amorphous phases. The elemental analysis of the surface of untreated S235 and oxidized steel S235 can be seen in the EDS and XPS experiments (Figure S1, Table S1, Figure S2), which showed that iron is dominating the outer sphere of all samples investigated. Regarding the cationic distribution derived from XPS investigation (Table S1) we can see that the Fe content on the surface of sample 1 exceeds 99% and is exactly on the level of the reference sample. The Mn content of sample 1 on the surface is 0.84% and exceeds the Mn content of the reference sample (0.53%). The EDS spectra (Figure S1) do not show un-expected findings. The dominating signals are as expected FeK_α and FeK_β besides FeL_α and OK_α. The Mn concentration on the surface of sample 1 is below the detection limit. EDS spectra of sample 1 showed no hints of a Cl contamination on the surface, i.e. no ClK_α peak could be obtained. Notably, prior and after long term chronopotentiometry for 50000 s at 2 mA/cm^2 current density in 0.1 M KOH the samples showed the same findings in the XPS and EDS experiments. High resolution XPS spectra should determine which iron or manganese compound is the dominant Mn/Fe species on or close to the surface, and even if this compound does not directly represent the catalytic active species itself then at least it presents the precursor for the catalytic active species (Figure S2). The Mn $2p_{3/2}$ and Fe $2p_{3/2}$ positions of several of the reference compounds are indicated by grey vertical bars [71, 72, 73].

A trivalent valence state was assigned to iron, situated in or close to the surface of all surface oxidized samples and of the reference sample. Derived from the Fe 2p3/2 binding energy, and the energetic position and shape of the charge transfer satellites most likely Fe_2O_3, besides small amounts of

FeO(OH) (signal at somewhat higher binding energy) have been formed on the surface of sample 1. With increasing chlorine exposure time (190, 500 and 720 min) the position of the envelope (~ 711 eV) of Fe $2p_{3/2}$ of the corresponding specimen 2, 3 and 4 is shifted towards higher binding energy. We therefore assume that the FeO(OH)/Fe_2O_3 ratio on the surface of the corresponding specimen shifts with increasing chlorine exposure time in favor of FeO(OH), for example from sample 1 to 4 the FeO(OH) content increases. As a consequence Fe_2O_3 seems to have superior electrocatalytic OER properties when compared with FeO(OH) in both, alkaline and neutral regime, because, as will be shown in the following sections 1.1.4 and 1.2, the overall electrocatalytic OER performance of sample 1 at pH 13 and pH 7 was significantly higher than that of samples 2, 3 and 4 achieved at significant longer exposure to Cl_2 (Table 1, Figure 3, Figure 4, Figure 6 d-f). Because of rather low Mn concentrations in between 0.37 and 0.84% (Table S1), and-, hence- the required long acquisition times for high resolution spectra our XPS investigation is limited to Mn 2p core level spectra of sample 1 and the reference sample. Despite the rather poor signal to noise ratio we can exclude any major contribution of metallic Mn at the surfaces of both samples. In particular the surface layers of sample 1 could contain some Mn^{2+} contributions, but the dominant oxidation state of manganese in, or close to, the surface seems to be +3 for both samples suggesting either MnO(OH) or Mn_2O_3 as the most likely Mn(III) compound on the surface of sample 1.

When comparing the Mn XPS spectra (Figure S2) of both samples (reference + sample 1) in detail it is noticeable that the Mn_2O_3 to MnO(OH) ratio for sample 1 is significantly higher than that for the untreated steel. Based on this we can assume that at both, pH 7 and pH 13 Mn_2O_3 shows superior OER activity when compared to MnO(OH). This agrees particularly well with recent findings by Zhou et al. [25] or Ramirez et al. [76] who reported on Mn_2O_3 species as the most active electrocatalytic Mn containing compounds with respect to OER. Based on the cationic distribution (Table S1) the surface of sample 2 (0.37%) contains less Mn than the surface of sample 1 (0.84%). We speculate that this and the higher FeO(OH)/Fe_2O_3 ratio for sample 2 when compared to sample 1 could be the origin of slightly higher OER activity of sample 1.

Thus to sum up the XPS spectra (Figure S2) could be reasonably resolved with the proviso that Fe_2O_3, FeO(OH), MnO(OH) and Mn_2O_3 are the predominant Fe- respectively Mn- compounds on the surface of the oxidized steel S235.

The findings of other groups

Unfortunately in recent literature it seems that it has been failed to recognize that already more than 35 years ago layers consisting of metal oxide species have been achieved via anodic deposition [74,56] and as early as 1983 electrodeposited Fe containing thin films were used for electrochemically initiated oxygen evolution reactions [57]. However, to the best of our knowledge, the active site for oxygen evolution on iron-oxide based surfaces of films or oxidized metal bodies could not be unequivocally identified until recently [76, 58]. Although critically instable Lyons and Brandon[75] found evidence that Fe(VI) species

play a role as active OER centers in electrocatalytic initiated OER on Fe electrodes performed in alkaline media. There indeed exists a sufficient amount of polarization data for electro-oxidized iron electrodes and based on this, reasonable OER mechanisms as well as active Fe species at intermediate OER stages like e.g. hydrated forms of Fe_2O_3 and FeO(OH) were suggested [38].

Recently published work focuses on electrochemically initiated water splitting on manganese oxide dominated surfaces particularly under neutral conditions [55, 76]. The evaluation of *in-situ* OER current measurements plus optical absorption experiments suggests that electron injection upon H_2O to MnO_2 resulted in trivalent Mn species, which acted as a direct precursor for O_2 evolution [55,]. To elucidate the structure-function relationship of the OER on Mn based electrocatalysts Ramirez et. al. investigated in their comprehensive study α–Mn_2O_3 besides Mn_3O_4 and MnO_x as prospective OER electrocatalysts in alkaline and neutral media. In their study α–Mn_2O_3 proved to be the catalyst of choice among these compounds in both, alkaline and neutral regime [76].

Thus our findings regarding the electrocatalytic active OER centers in Mn/Fe oxide containing layers line up very well with earlier investigations [28, 38,55, 76]. However due to a general lack of studies providing spectroscopic- and thermodynamic data the OER catalytic centers are still controversial discussed.

1.1.4 The influence of the chlorine exposure time on surface composition and OER properties

Figure 3 presents the CVs of samples 1-4 and of the untreated S235 reference sample measured in 0.1 M KOH. The curve form of the CVs of all samples closely resembles those of untreated or pre-reduced metals such as Ni, Fe or Co [38]. However, the onset of OER on the surface of samples 1-4 is negatively shifted with an onset of OER close below 1.5 V vs. RHE, in comparison with the onset of oxygen evolution on untreated steel S235 or pure iron. The differences between the surface compositions of the samples exposed to Cl_2 for different durations (Table S1; See also section 2.1.2) are small, and we did not obtain a clear shift of the composition towards a defined direction with e.g. increasing chlorine exposure time. Only for sample that was exposed to Cl_2 for 9 hours a weak Cl contamination can be seen in the spectra taking the form of a weak ClK_α peak (Figure S1, sample 4). We recently showed that chlorination of stainless steel resulted in a suppression of Ni and a Cr enrichment on, or close to, the surface [48]. This in contrast to the findings presented here led to significant changes of the cationic distribution within the surface. If chlorination of S235 steel has not affected the cationic distribution, then it could in principle have resulted in the formation of metal chlorides on the surface, which then once in contact with aqueous solution dissociates to give chloride ions in aqueous solution that in turn falsifies the results. While recording CV plots Cl_2 evolution reaction could potentially have taken place. However we clearly assign the obtained current to the oxygen evolution principally for two reasons:

1. No chloride ions could be found in the rinsing water (Cl−ion with $AgNO_3$ solution showed no precipitation) after cleaning the specimen.
2. Taken into consideration that electrolysis of NaCl in alkaline regime leads to the formation of hypochlorite and chlorate if the formed Cl_2 is not separated from OH^- [77] during electrochemical measurements any theoretically formed chlorine should react in alkaline solution to give binary Cl-O species. But none of them could be found in the electrolyte after completion of the electrochemical scans (See supporting information's).

A direct comparison of the CVs belonging to the reference sample and to samples 1-4 gives an impression about how the non- steady state OER properties of steel S235 could be improved upon chlorination. The gap is especially substantial between curves attributed to the reference sample and sample 1 (Figure 3a, b): There is on the one hand a significant negative horizontal shift of the curve by around 70 mV, and in addition the CV of sample 1 was found to be stiffer than that of the reference sample. This can, in our opinion only be explained by a change of the chemical nature of the surface of the samples during the surface treatment. An enhancement of the active area would solely lead to a vertical shift of the curve to higher current values. Notably, both effects were found to be reduced for samples which were exposed to chlorine for more than 110 min, i.e. for samples 2 (190 min exposure time), respectively 3 and 4 (500 min and 720 min exposure time). As such the fact that with an extension of the chlorination exposure time the electrochemical properties deteriorated progressively (Figure 3 b, c, d) is likely to be caused by a higher FeO(OH) content on the surface of the samples exposed to chlorine for longer than 110 min (See section 2.1.3). This result of the non-steady state measurements agrees well with the results derived from steady state measurements (Figure 4a-d). The overpotential for the OER in 0.1 M KOH at 2 mA/cm^2 current density derived from long term chronopontentiometry plots was found to be significantly decreased when comparing the reference sample (462 mV) with sample 1 (347 mV; Figure 4b), but for samples exposed to Cl_2 for more than 110 min the overpotential increased. This is expected, particularly when taken into consideration the results of the non-steady state measurements, with increasing duration of the chlorination (sample 2:362 mV; Figure 4c; Sample 3:382 mV; Figure not shown; Sample 4: 390 mV; Figure 4d). Nevertheless these values represent a reinforced electro catalytic performance when compared with the corresponding key data of pure iron [49, 50, 66]. Also the stability of all samples under alkaline catalysis conditions was found to be surprisingly good. After 50000 s the potential required for 2 mA/cm^2 current density did not significantly change (Figure 4b, c, d). In case of sample 2 the potential was even below the start value of 1.6 V vs. RHE. Due to the strong stability of the catalyst in alkaline medium the value of the overpotential of sample 1, 2 and 4 derived from the chronopotentiometry plot (347 mV, 362 and 390) performed in 0.1 M KOH at 2 mA/cm^2 current density can be quite well verified via the CV measurement (Figure 3 b, c, d, ~ 352 mV (1), 357

mV (2), 380 mV (4)). In this case it should be allowed to estimate (extrapolate) overpotentials on the basis of CV measurements. The estimated overpotential of sample 1 at 3 mA/cm^2 is around 357 mV (Figure 3b) and lines up perfectly with the values derived from chronopotentiometry at 2 mA cm^{-2} (Figure 4b:347 mV) respectively at 10 mA cm^{-2} (Figure S4: 416 mV). The estimated overpotentials of samples 2 and 4 in 0.1 M KOH at 3 mA/cm^2 amounted to 372 mV, 389 mV respectively (Figure 3c, d). Chlorination of steel for 110-200 min resulted in oxide layers around 2-6 microns in thickness (Figure 5, sample 1, 2). Under extended duration of chlorination the oxide layer further grows and the thickness can reach up to 24 microns (sample 3, Figure 5). The thickness of the oxide layer can strongly vary even within one sample (Figure 5) and sample 4 showed although achieved after the longest exposure time within our samples series a layer thickness (~ 8 microns) below the value of sample 3. Groups who anodized metals or alloys in order to improve the OER properties found that the overpotential for the oxygen evolution decreased with increasing anodizing time [43, 46, 78]. This increase is due to the growth of an electrocatalytically active oxide layer on the alloy. Interestingly in our study the thicker layers achieved after longer chlorination time (sample 3: 500 min, sample 4: 720 min) did not result in better OER performance at pH 13 (Figure 5). Quite the contrary, the potential necessary to guarantee a 2.0 mA/cm^2 current density in 0.1 M KOH during long term chronopotentiometry was found to be substantially increased for samples exposed to chlorine for more than 6 hours (sample 3:382 mV, Figure not shown; Sample 4: 390 mV, Figure 4d). Particularly sample 4 shows poor current density in high potential regime (Figure 3d). A current density of 5 mA/cm^2 could not be achieved even at 1.65 V vs. RHE (Figure 3d). However all chlorinated samples proved to be stable water splitting electrocatalysts even after tens of hours operation time, and regarding the long time stability at least under catalysis conditions in alkaline medium, the thickness of the layer respectively the duration of the Cl_2 treatment played no major role.

The long-term performance of steel type alloys for oxygen evolution in alkaline regime has very rarely been investigated which definitely hampers any comparison of our data with other, published samples. Marian Chatenet et al. investigated long-time polarization of unmodified stainless steel 316L and obtained a sufficient stability within operation times of more than 1000 hours [45].

1.2 **Properties of chlorinated steel S235 in neutral regime**

The basic concept of using renewable energy sources like wind energy for the electrocatalytic conversion of e.g. seawater into cleavage products oxygen and hydrogen has pushed the development of efficient electrocatalysts for the oxygen evolution in neutral media. Besides, chloride ion contamination (most natural water resources contain chloride salts which is considered as a serious obstacle), water splitting under neutral conditions was previously hampered by substantially higher overpotentials for the OER on metal anodes [48] when compared with water splitting under alkaline conditions. Therefore state

of the art electrocatalysts should prove their suitability as an efficient OER catalyst in both, alkaline and neutral media. A direct comparison of the CV curve of the untreated steel S235 (Figure 6a) with the corresponding curve of sample 1 (Figure 6b) reveals the efficiency of the surface modification of steel S235 by chlorination with respect to the water splitting properties in neutral regime. Whereas the current density at maximum potential within the CV plot (1.25 V–IR vs. Ag/AgCl) is 0.85 mA/cm^2 in case of the untreated steel (Figure 6a), the corresponding values for the chlorinated samples exceeds 1.6 mA (sample 1:Figure 6b; Sample 3: Figure S6a) respectively 2 mA for sample 2 (Figure S7). Untreated steel S235 initiates anodic water-splitting in neutral medium at potentials higher than 1.12 V vs. Ag/AgCl which can be taken from the abrupt current increase at a potential around 1.12 V (Figure 6a). The onset of water splitting at pH 7 is shifted for all chlorinated samples to lower potentials, e.g. for sample 1 by around 100 mV (Figure 6a, 6b), and for the samples 2, 3 and 4 by around 110 mV (Figure S7, S6a, S8). In our view this horizontal shift can just as in the case of the shift of the corresponding CVs recorded in alkaline regime only be explained by a change of the chemical nature of the surface. The efficiency of the chosen surface modifications for improving the electrocatalytic water splitting properties in neutral conditions was confirmed not only by non-steady state measurements, but also by steady state techniques. The Tafel line of sample 1 was substantially negatively shifted (~100 mV) when compared with the Tafel line of the reference sample (Figure 6c). In addition, the Tafel slope assigned to sample 1 (172.4 mV dec^{-1}) was significant smaller than the one assigned to the reference sample (201.9 mV dec^{-1}). Tafel slopes of OER electrocatalysts determined in pH 7 solutions have rarely been published. Very recently graphene-Co_3O_4 nanocomposites and ZrS_3 nanosheets were reported as prospective OER electrocatalysts for water splitting under neutral and alkaline conditions showing Tafel slopes of 98 mV dec^{-1} respectively 102 mV dec^{-1} in 0.1 M phosphate buffer solution [61,28]. Chronopotentiometry data demonstrate the very high stability of our samples 1, 2 and 4 under working conditions (0.1 M KH_2PO_4/K_2HPO_4 pH 7 solution; 1 mA total current), (Figure 6d-f). These samples behave remarkably stable under electrolysis condition in neutral regime even after operation times of up to 180000 s. The untreated alloy showed at pH 7 so poor electrocatalytic activity that we failed to reach 1 mA total current at reasonable potentials. The overpotential for the OER on our surface oxidized steel S235 samples determined in pH 7 corrected 0.1 M KH_2PO_4/K_2HPO_4 at 1 mA/cm^2 current density amounted to 462 mV (Sample 1), 512 mV (Sample 2), 598 mV (Sample 3), 602 mV (Sample 4) respectively (Figure 6d,e , S6b, 6f). Chlorination of S235 steel for 110 min resulted in an OER electrocatalyst with the lowest overpotential within our samples series. Extension of the Cl_2 exposure led to higher overpotentials, i.e. for durations of chlorination > 110 min the overpotential of the corresponding increased with increasing chlorination period. The same dependence was found to be valid at pH 13 (See section 2.1.4, Figure 4) and therefore we believe that a shift of the Fe_2O_3/FeO(OH) ratio on the surface (section 2.1.3) also explains this result.

Generally metal oxides are considered to be instable as oxygen-evolution electrocatalysts in neutral and particularly in acidic regime and only a few catalysts operate in neutral water under ambient conditions. Electrodeposited FeO(OH) [56, 57] besides cobalt-phosphate compound [6,53] are among the few known non noble compounds for which sufficient activity and acceptable stability during water splitting at neutral pH has been demonstrated [53] . We recently reported on surface oxidized AISI 304 steel (Cr-Ni stainless steel) as a prospective anode material for OER in alkaline and neutral regime [48]. Here, as mentioned, the OER activity found at pH 13 was superior to the activity of the samples discussed in the current report. However chlorinated AISI 304 [48] showed in comparison with chlorinated S235 in neutral phosphate buffer a poorer OER activity as can be seen from the overpotential of 500 mV at 0.65 mA/cm^2 current density in 0.1 M KH_2PO_4/K_2HPO_4 solution [48]. An overpotential of 480 mV at pH 7 and at 1 mA/cm^2 current density was very recently reported for electrodeposited iron based thin films [58].

In summary: Surface oxidation of S235 steel upon straightforward chlorination converted this very cheap and commodity starting material into a robust, efficient and highly competitive OER electrocatalyst exhibiting OER key data (462 mV overpotential at 1 mA/cm^2 current density) on the same level as those shown by recently developed highly advanced state of the art electrocatalysts.

2 **Conclusion**

The generation of solar fuels via the conversion of water into its cleavage products hydrogen and oxygen photo- or electrocatalytically realized by using renewable energy sources will help to overcome the limited availability of fossil fuels for future applications. Thus the optimization of the evolution reactions occurring on both, the cathode and on the anode is and will continue to be of great importance. Particularly the development of earth abundant, cost effective OER electrocatalysts with appropriate characteristics regarding catalytic activity and stability in neutral media is known as a future challenge of highest significance as it could be a part of a concept that basically covers seawater-splitting using renewable energy sources. The current work we present evaluates the suitability of surface oxidized steel S235 as prospective anode material for the electrocatalytic initiated oxygen evolution reaction in both, alkaline and in neutral media. The electrocatalytic properties of the material were enhanced significantly by applying an oxidation of the surface using humid Cl_2 gas. The best electrocatalytic properties were achieved when the samples were exposed to Cl_2 gas for 110 min resulting in an ~ 2 micrometer thick Fe-Mn-oxide layer firmly attached to the substrate, converting the standard carbon manganese steel into an oxygen evolution electrocatalysts. This catalyst works efficiently in neutral 0.1 M KH_2PO_4/K_2HPO_4 solution as demonstrated by the low overpotential for the OER (462 mV at 1 mA/cm^2 current density) at pH 7. Very likely the iron-manganese-oxide layer of the metal-oxide composite is responsible for the reduction of the overpotential of the oxidized steel samples and protects the metal underneath the layer

for further (inner) oxidation leading to sufficient stability under catalysis conditions. Even after 100000 s of chronopotentiometry carried out at 1 mA/cm^2 current density in neutral phosphate buffer solution the catalytic properties remained on the start level. Thus, while the OER properties of chlorinated steel S235 in neutral medium were more than satisfactory the corresponding characteristics in 0.1 M KOH are not nearly at the level of either noble metal containing electrocatalysts or state of the art water-splitting catalysts such as mixed spinel oxides, perovskite-type compounds or surface modified stainless steel. Under optimized conditions chlorinated S235 exhibited in 0.1 M KOH a stable current density of 2.0 mA/cm^2 at 347 mV overpotential, of 10 mA/cm^2 at 447 mV overpotential respectively. The Faradaic efficiency amounted to 67% after 3000 s of chronopotentiometry at 2.0 mA/cm^2 current density in 0.1 M KOH.

We consider the surface modified steel S235 suitable as an OER electrode for the conversion of neutral medium (pH 7 buffer solution) into oxygen as a meaningful outcome taken into consideration the low overpotential and sufficient catalytic stability for the OER as well as the low cost of both, the material and the surface treatment. We strongly believe that surface modification of steel that contains so many interesting ingredients not only with respect to OER electrocatalysis is a promising approach on the way to develop affordable alternatives to recently developed advanced functional materials

3 Materials and Methods

Sample	Electrode area(cm^2)	Distance between RE and WE (mm)	Electrolyte	Eletrolyte resistance (Ω)	Voltage drop (mV)**
1-4	1.5	1	0.1 M KOH	5*	15
Reference	1.5	1	0.1 M KOH	5*	15
IrO_2-RuO_2	2	1	0.1 M KOH	5*	15
1-4	1.5	3	pH 7 buffer	20.4**	30.6
Reference	1.5	3	pH 7 buffer	20.4**	30.6

Table 2. Key data of the (three electrode) electrochemical set up used for measurements in alkaline regime (0.1 M KOH) and in pH 7 buffer (0.1 M KH_2PO_4/K_2HPO_4). *50 Ω ≙ 10 mm; * Chronopotentiometry-/Tafel measurements performed in 0.1 M KOH at 2 mA/cm^2 current density.

**68 Ω ≙ 10 mm; ** Chronopotentiometry-/Tafel measurements performed in 0.1 M KH_2PO_4/ K_2HPO_4 at 1 mA/cm^2 current density.

3.1 Preparation of the samples

Surface oxidation of stainless steel via Chlorine gas (samples 1-4)

All samples with a total geometry of 100x10x1,5 mm were constructed from 1,5 mm thick Steel S235. Pre-treatment: Prior to each surface modification the surface of the metal was cleaned intensively with ethanol and polished with grit 600 SiC sanding paper. Afterwards the surface was rinsed intensively with deionized water. Cl_2 gas was generated immediately before usage via oxidation of aqueous solution of HCl with $KMnO_4$. In a 25 ml Erlenmeyer flask 0,5 g (3.15 mmol) $KMnO_4$ (VWR, Darmstadt) was dissolved under stirring in 12 ml deionized water and 150 mg 37 wt.%, (1.52 mmol) HCl (VWR, Darmstadt) was added at ambient temperature. Subsequently the steel samples were positioned within the opening and the $KMnO_4$/HCl reaction mixture was stirred during activation at room temperature. The duration of the surface treatment was varied according to Table 1 between 110-720 min. After chlorination the samples were rinsed intensively with tap water for 15 min and afterwards with deionized water for an additional 10 minutes. No chloride ions could be detected in the rinsing water (Cl^-ion with $AgNO_3$ solution showed no precipitation). Prior to the electrochemical characterization the samples were dried under air at ambient temperature. Each of the experiment was repeated three times.

3.2 **Catalyst Characterization**

Electrochemical Measurements

A three electrode set-up was used for all electrochemical measurements. The working electrode with a total geometry of 100x10x1,5 mm was constructed from 1,5 mm thick Steel S235 on which an apparent surface area of ~ 1.5 cm^2 was defined by an insulating tape (Kapton tape). A platinum wire electrode (2x2 cm geometric area) was employed as the counter electrode. Cyclic Voltammograms (CV) were recorded under stirring (180 r/min) using a magnetic stirrer (15 mm stirring bar). The scan rate was set to 20 mV/s and the step size was 2 mV. Chronopotentiometry scans were recorded under stirring (180 r/min) using a magnetic stirrer (20 mm stirring bar). For all measurements the reference electrode was placed in between the working and the counter electrode. The distance between the working electrode and the reference electrode was adjusted to 1-3 mm and the distance between the reference electrode and the counter electrode was adjusted to 4-5 mm. All electrochemical data were recorded digitally using a Potentiostat Interface 1000 from Gamry Instruments (Warminster, PA 18974, USA) which was interfaced to a personal computer. As IR compensation via standardized software was found to be too strong, i.e. leading to anomalous voltage-current behavior (curves in CV plots) at high potentials. We corrected Ohmic losses manually by subtracting the Ohmic voltage drop from the measured potential on the basis of a electrolyte (0.1 M KOH) resistance of 50 Ω at 10 mm electrode distance, 68 Ω at 10 mm electrode distance respectively (See Table 2). IR-corrected potentials are denoted as E-IR.

Electrochemical measurements in alkaline medium

A reversible hydrogen reference electrode (RHE, HydroFlex, Gaskatel Gesellschaft für Gassysteme durch Katalyse und Elektrochemie mbH. D-34127 Kassel, Germany) was utilized as the reference standard, therefore all voltages are quoted against this reference electrode. The measurements were performed in a 0.1 M KOH solution (Merck TitriPur). The potential was cycled between 1 and 1.7 V vs. RHE. Chronopotentiometry scans were conducted at a constant current of 3 mA (current density: 2.0 mA/cm^2).

Electrochemical measurements in neutral medium

A Ag/AgCl electrode (Metrohm, 70794 Filderstadt, Germany) was utilized as the reference standard, therefore voltages are quoted against this reference electrode. Long time chronopotentiometry was performed while using a reversible hydrogen reference electrode (RHE, HydroFlex, Gaskatel Gesellschaft für Gassysteme durch Katalyse und Elektrochemie mbH. D-34127 Kassel, Germany) as the reference. For the measurements at pH 7 a solution of 0.1 M KH_2PO_4/K_2HPO_4 (VWR, minimum 99% purity) in Millipore water (resistivity > 18 MΩ cm) was used. CVs were recorded while the potential was cycled between 0.4 and 1.25 V vs. Ag/AgCl. Stability scans were conducted in chronopotentiometry mode at a constant current of 1.5 mA (current density: 1 mA/cm^2).

XPS Spectroscopy

In addition to Energy-disperse X-Ray spectroscopy (EDS) performed on the surface of all samples within the SEM experiments (Figure S1) the composition of the surface of samples 1, 2 and 4 as well as the untreated S235 steel was determined by X-Ray photoelectron Spectroscopy (XPS; Table S1). High resolution XPS spectra of the reference sample as well as of samples 1-4 can be taken from Figure S2. XPS measurements were performed using a PHI 5600ci multiutechnique spectrometer equipped with a monochromatic Al Kα source with 0.3 eV full width at half-maximum. The overall resolution of the spectrometer is 1.5% of the pass energy of the analyzer, 0.7 eV in the present case. The measurements were recorded with the sample at room temperature. The spectra were calibrated with a corresponding measurement of the Au $4f_{7/2}$ level (84.0 eV) of a gold foil. As to the evaluation of the cationic composition of the samples, a standard Shirley background is subtracted from all spectra. The relative elemental Fe and Mn concentration were determined using the PHI sensitivity factors (see Table S1) included in the PHI Multipak program package.

Electron microscopic experiments

Determination of the thickness of the oxide layer

For the oxide layer thickness determination, the specimens were covered by an aluminum foil in order to protect the oxide layer during specimen preparation. For the mechanical preparation of cross-sections a conductive resin suitable for SEM was used. Specimens were ground and polished (final polishing step:

3μm diamond suspension). Etching of specimens was not necessary. SEM was performed employing a Zeiss DSM 962. The oxide layer thickness was measured in SEM-images obtained in BSE-modus.

X-ray diffraction

X-ray patterns of the oxidized samples were obtained by theta/2 theta scans measured in reflection using a PANalytical X'Pert Pro MRD diffractometer equipped with an Eulerian cradle, which was operated with Cu Kα radiation at 40 kV and 40 mA.

Supporting Information

Additional cyclo voltamograms and chronopotentiometry scans as well an EDS spectra of the oxidized surface of the steel samples and a table showing the cationic distribution of Mn and Fe can be taken from the Supporting Information.

Figure 1

Figure 1. Steady State performance of sample 1. **(a) Long time chronopontentiometry** scan of sample 1 in 0.1 M KOH at 2.0 mA/cm^2 (total current: 3 mA). Average overpotential within 100000 s plot: 347 mV at 2.0 mA/cm^2. **(b) Top panel:** Correlation of oxygen evolution of sample Elox300 in 0.1 M KOH (black curve) determined with an optical dissolved oxygen (OD) sensor using the so-called fluorescence quenching method with the charge passed through the electrode system (red line corresponds to 100% Faradaic efficiency). Lower panel: Corresponding chronopotentiometry plot. Current density: 2 mA/cm2; Average Overpotential within the 3000 s plot: 360 mV. The electrode area was 1.5 cm^2. Amount of the electrolyte: 0.4 l; Start value of dissolved oxygen: 0.08 mg/l (t= 0 s); End value of dissolved oxygen (t = 3000 s): 1.33 mg/l (nominal value (100%):1.946 mg/l). Faradaic efficiency of the OER after 3000 s runtime: 67 %. **(c) Tafel plots of sample 1** and IrO_2-RuO_2 determined in 0.1 M KOH. Average voltage values for the Tafel plots were derived from 200 second chronopotentiometry scans at the corresponding current densities. IR compensation was performed for all plots taking into account the values for electrolyte resistance from Table 2. The electrode area was 1.5 cm^2 (sample 1, respectively 2 cm^2 (IrO_2-RuO_2)). **(d) Tafel plots** of sample 1 and the reference sample determined in 0.1 M KOH. Average voltage values for the Tafel plots were derived from 200 second chronopotentiometry scans at the corresponding current densities. IR compensation was performed for all plots taking into account the values for electrolyte resistance from Table 2.

Figure 2

Figure 2. Kinetic parameters of the OER on the surface of oxidized steel S235. **(a) Comparison** of the Tafel lines of sample 1 determined in 0.1 M and 2 M KOH. Average voltage values for the Tafel plots were derived from 200 second chronopotentiometry scans at the corresponding current densities. IR compensation was performed for all plots taking into account the values for electrolyte resistance from Table 2. **(b) The dependence** of the logarithm of the current density (A cm^{-2}) from the logarithm of the

OH^- activity at constant temperature of 298 K and constant potential of 1.55 V *versus* RHE (∂ log i/∂ log a)$_E$ at E=1.55 V and T=298 K). The slope amounted to 0.462. (c) **The dependence** of the logarithm of the current density (A cm^{-2}) from the logarithm of the OH^- activity at constant temperature of 298 K and constant potential of 1.59 V *versus* RHE (∂ log i/∂ log a)$_E$ at E=1.59 V and T=298 K). The slope amounted to 0.475.

Figure 3

Figure 3. Comparison of the non-steady state electocatalytic properties of the reference sample as well as samples 1,2 and 4 determined in 0.1 M KOH; Scan rate: 20 mV/s; Step size: 2 mV. **(a) Cyclic voltammogram** of the reference sample in 0.1 M KOH. **(b) Cyclic voltammogram** of sample 1 in 0.1 M KOH. Estimated overpotential: 357 mV at 3 mA/cm^2 current density. **(c) Cyclic voltammogram** of sample 2 in 0.1 M KOH. Estimated overpotential: 372 mV at 3 mA/cm^2 current density. **(d) Cyclic voltammogram** of sample 4 in 0.1 M KOH. Estimated overpotential: 389 mV at 3 mA/cm^2 current density.

Figure 4

Figure 4. Comparison of the steady state electocatalytic properties of the reference sample , respectively samples 1,2 and 4 determined in 0.1 M KOH. **(a) Chronopontentiometry** scan of the reference sample in 0.1 M KOH at 2.0 mA/cm^2 (total current: 3 mA). Average overpotential (100000 s): 462 mV. **(b) Long time chronopontentiometry** scan of sample 1 in 0.1 M KOH at 2.0 mA/cm^2 (total current: 3 mA). Average overpotential (100000 s): 347 mV at 2.0 mA/cm^2. **(c) Long time chronopontentiometry** scan of sample 2 in 0.1 M KOH at 2.0 mA/cm^2 (total current: 3 mA). Average overpotential (50000 s): 362 mV at 2.0 mA/cm^2. **(d) Long time chronopontentiometry** scan of sample 4 in 0.1 M KOH at 2.0 mA/cm^2 (total current: 3 mA). Average overpotential (100000 s): 390 mV at 2.0 mA/cm^2.

Figure 5

Figure 5. SEM images of transversely cuts of samples 1-4. Area A: steel substrate. Magnification: 3000x (samples1, 2, 4) and 1000x (sample 3); area B: oxide layer; area C: aluminum (from sample preparation).

Figure 6

Figure 6. Comparison of the non-steady state and steady state electocatalytic properties of the reference sample as well as samples 1,2 and 4 determined at pH 7 in 0.1 M KH_2PO_4/K_2HPO_4. **(a) Cyclic voltammogram** of the reference sample at pH 7 in 0.1 molar KH_2PO_4/K_2HPO_4. Scan rate: 20 mV/s; Step size: 2 mV. **(b) Cyclic voltammogram** of sample 1 at pH 7 in 0.1 molar KH_2PO_4/K_2HPO_4. Scan rate: 20 mV/s; Step size: 2 mV. **(c) Comparison** of the Tafel lines of sample 1 and the reference sample determined in 0.1 M KH_2PO_4/K_2HPO_4. Average voltage values for the Tafel plots were derived from 200 second chronopotentiometry scans at the corresponding current densities. IR compensation was performed for all plots taking into account the values for electrolyte resistance from Table 2. **(d) Long time Chronopotentiometry** of sample 1 in 0.1 M KH_2PO_4/K_2HPO_4 at 1 mA/cm^2 (total current: 1.5 mA). Average overpotential: 462 mV within 100000 s. **(e) Long time Chronopotentiometry** of sample 2 in 0.1 M KH_2PO_4/K_2HPO_4 at 1 mA/cm^2 (total current: 1 mA). Average overpotential: 512 mV within

100000 s. **(f) Long time Chronopotentiometry** of sample 4 in 0.1 M KH_2PO_4/K_2HPO_4 at 1 mA/cm^2 (total current: 1 mA). Average overpotential: 602 mV within 100000 s.

Notes and references

[1] M. G. Walter, E. L. Warren, J. R. McKone, S. W. Boettcher, Q. Mi, E. A. Santori, N. S. Lewis, *Chem. Rev*., **2010**, *110*, 6446.

[2] T. R. Cook, D. K. Dogutan, S. Y. Reece, Y. Surendranath, T. S. Teets, D. G. Nocera, *Chem. Rev*., **2010**, *110*, 6474.

[3] A. J. Bard, M. A. Fox, *Acc. Chem. Res.,* **1995,** *28,* 141.

[4] O. Merka, D. W. Bahnemann, M. Wark, *Catalysis Today,* **2013**, *225,* 102.

[5] M. T. M. Koper, *J. Electroanal. Chem.,* **2011**, *660,* 254.

[6] M. W. Kanan, D. G. Nocera, *Science,* **2008**, *321,* 1072.

[7] Y. Gorlin, T. F. Jaramillo, *J. Electrochem. Soc.,* **2012**, *159,* H782.

[8] T. Reier, M. Oezaslan, P. Strasser, *ACS Catal.,* **2012**, *2,* 1765.

[9] K. C. Neyerlin, G. Bugosh, R. Forgie, Z. Liu, P. Strasser, *J. Electrochem. Soc.,* **2009**, *156,* 3, B363.

[10] Y. Lee, J. Suntivich, K. J. May, E. E. Perry, Y. Shao-Horn, *J. Phys. Chem. Lett.,* **2012**, *3,* 399.

[11] Y. Gorlin, T. F. Jaramillo, *J. Am. Chem. Soc.,* **2010**, *132,* 13612.

[12] S. Trasatti, *Electrochim. Acta,* **1984**, *29,* 1503.

[13] S. Trasatti, *Electrochim. Acta,* **1987**, *32,* 369.

[14] S. Trasatti, *Electrochim. Acta,* **2000**, *45,* 2377.

[15] V. Petrykin, K. Macounova, O. A. Shlyakhtin, P. Krtil, *Angew. Chem. Int. Ed.,* **2010**, *49,* 4813.

[16] T. Nakagawa, C. A. Beasley, R. W. Murray, *J. Phys. Chem. C.,* **2009**, *113,* 12958.

[17] Y. Zhao, E. A. Hernandez-Pagan, N. M. Vargas-Barbosa, J. L. Dysart, T. E. Mallouk, *J. Phys. Chem. Lett.,***2011**, *2,* 402.

[18] M. E. G. Lyons, S. Floquet, *Phys. Chem. Chem. Phys.,* **2011**, *13,* 5314.

[19] H. Nhan Nong, H.-S. Oh, T. Reier, E. Willinger, M.-G. Willinger, V. Petkov, D. Teschner, P. Strasser, *Angew. Chem. Int. Ed.*, **2015**, *54,* 2975.

[20] J. Soldat, R. Marschall, M. Wark, *Chemical Science,* **2014**, *5,* 10, 3746.

[21] J. P. Hoare, In *Advances in Electrochemistry and Electrochemical Engineering*; Delahay, P.; Tobias, C. W.; Interscience, New

York, **1966**, **Vol. 6**, p 201-288.

[22] A. C. C. Tseung, S. Jasem, *Electrochim. Acta,* **1977***, 22,* 31.

[23] M. Pourbaix, In *Atlas d`Equilibres Electrochemiques a 25 °C.* Gauthiers-Villars, Paris (1963).

[24] M. S. El-Deab, M. I. Awad, A. M. Mohammad, T. Ohsaka, *Electrochem. Commun.,* **2007**, *9,* 2082.

[25] F. Zhou, A. Izgorodin, R. K. Hocking, L. Spiccia, D. R. MacFarlane, *Adv. Energy Mater.,* **2012**, *2,* 1013.

[26] J. O`M. Bockris, T. Otagawa, *J. Phys. Chem.,* **1983,** *87,* 2960.

[27] J. O`M. Bockris, T. Otagawa, *J. Electrochem. Soc.,* **1984***, 131,* 290.

[28] Y. Zhao, S. Chen, B. Sun, D. Su, X. Huang, H. Liu, Y. Yan, K. Sun, G. Wang, *Sci. Rep.* 2014, *5,* 7629, DOI: 10.1038/srep07629.

[29] C. R. Davidson, K. Kissel, S. Srinivasan, *J. Electroanal. Chem.,* **1982**, *132,* 129.

[30] J. Suntivich, K. J. May, H. A Gasteiger, J. B.Goodenough, Y. A. S.-Horn, *Science,* **2011**, *334,* 1383.

[31] A. Grimaud, K. J. May, C. E. Carlton, Y.-L. Lee, M. Risch, W. T. Hong , J. Zhou, Y. Shao-Horn, *Nature Commun.,* **2013**, *4,* 2439, doi:10.1038/ncomms3439.

[32] S. Chen, S.-Z. Qiao, *ACSNano,* **2013**, *7,* 10190.

[33] H.-C. Chien, W.-Y. Cheng, Y.-H. Wang, T.-Y. Wie, S.-Y. Lu, *J. Mater. Chem.,* **2011**, *21,* 18180.

[34] W. Zhou, X.-J. Wu, X. Cao, X. Huang, C. Tan, J. Tian, H. Liu, J. Wang, H. Zhang, *Energy Environ. Sci.,* **2013**, *6,* 2921.

[35] V. K. Prasad Srirapu, C. Shekhar Sharma, R. Awasthi, R. Nath Singh, A. S. Kumar Sinha, *Phys. Chem. Chem. Phys.,* **2014**, 7385.

[36] N. Sato, N. G. Okamoto, *Electrochim. Acta,* **1965**, *10,* 495.

[37] M. H. Miles, G. Kissel, P. W. T. Lu, S. Srinivasan, *J. Electrochem. Soc.,* **1976**, *123,* 332.

[38] M. E. G. Lyons, M. P. A. Brandon, *J. Electroanal. Chem.,* **2010**, *641,* 119.

[39] X. Lu, C. Zhao, *Nature Commun.,* **2015**, *6,* 6616, 1-7.

[40] D. A Corrigan, *J. Electrochem. Soc.* **1987**, 134, 377.

[41] D. A. Corrigan, R. M. Bendert, *J. Electrochem. Soc.* **1988**, 135, C156−C156.

[42] J. Cerny, K. Micka, *J. Power Sources,* **1989**, *25,* 111.

[43] M. E. G. Lyons, R. E. Doyle, *Int. J. Electrochem. Sci.,* **2011**, *6,* 5710.

[44] K. C. Leonard, M. I. Tejedor-Anderson, M. A. Anderson, *Int. J. Hyd. Energy,* **2012**, *37,* 18654.

[45] F. Moureaux, P. Stevens, G. Toussaint, M. Chatenet, *J. Power Sources,* **2013**, *229,* 123.

[46] M. E. G. Lyons, R. L. Doyle, *Int. J. Electrochem. Sci.,* **2012**, **7**, 9488.

[47] M. E. G. Lyons, L. D. Burke, *J. Electroanal. Chem.,* **1984**, *170,* 377.

[48] H. Schäfer, S. M. Beladi-Musavi, L. Walder, J. Wollschlaeger, O. Kuschel, S. Ichilmann, S. Sadaf, M. Steinhart, K. Küpper, L. Schneider, *ACS Catal.,* **2015***, 5,* 2671.

[49] K. Lian, S. J. Thorpe, D. W. Kirk, *Electrochim. Acta,* **1992**, *37,* 169.

[50] T. Kessler, W. E. Triaca, A. Arvia, *J. Appl. Electrochem.,* **1994**, *24,* 310.

[51] H. Schäfer, S. Sadaf, L. Walder, K. Kuepper, S. Dinklage, J. Wollschlaeger, L. Schneider, M. Steinhart, J. Hardege, D. Daum, *Energy Environ. Sci.* **2015**, DOI:10.1039/C5EE01601K.

[52] K. N. Ferreira, T. M. Iverson, K. Maghlaoui, J. Barber, S. Iwata, *Science*, **2004**, 303, 1831.

[53] Y. Surendranath, M. Dinca, D. G. Nocera, *J. Am. Chem. Soc.,* **2009**, *131,* 2615.

[54] P. W. Menezes, A. Indra, N. R. Sahraie, A. Bergmann, P. Strasser, M. Driess, *ChemSusChem*, **2015**, 8, 164.

[55] T. Takashima, K. Hashimoto, R. Nakamura, *J. Am. Chem. Soc.,* **2012**, *134,* 1519.

[56] M. M. Lohrengel, P. K. Richter, J. W. Schultze, *Ber. Bunsenges. Phys. Chem.,* **1979**, 83**,** 490.

[57] J. W. Schultze, S. Mohr, M. M. Lohrengel, *J. Electroanal. Chem.,* **1983**, 154, 57.

[58] Y. Wu, M. Chen, Y. Han, H. Luo, X. Su, M.-T. Zhang, X. Lin, J. Sun, L. Wang, L. Deng, W. Zhang, R. Cao, *Angew. Chem. Int. Ed.,* **2015**, 54, 4870.

[59] F. Jiao, H. Frei, *Chem. Commun*., **2010**, *46,* 2920.

[60] M. M. Najafpour, *Dalton Trans.,* **2011**, *40,* 3805.

[61] J. Xie, R. Wang, J. Bao, X. Zhang,H. Zhang, S. Lib, Y. Xie, *Inorg. Chem. Front*., **2014**, 1, 751.

[62] J. He, Y. Peng, Z. Sun, W. Cheng, Q. Liu, Y. Feng, Y. Jaing, F. Hu, Z. Pan, Q. Bian, S. Wei, *Electrochim. Acta,* **2014**, *119,* 64.

[63] A. K. Greene, B. K. Few, J. C. Serafini, *J. Dairy Science,* **1993**, *76,* 3617.

[64] J. K. S. Tee, D. J. Fray, *Ironmaking Steelmaking,* **2005**, *32,* 509.

[65] Y. Qiu, L. Xin, W. Li, *Langmuir,* **2014**, *30,* 7893.

[66] A. T. Kuhn, D. Wakeman, E. Y. El Roubi, G. E. S. Collins, *Electrochim. Acta,* **1983**, *28,* 515.

[67] E Gileadi, Electrode Kinetics for Chemists, Chemical Engineers, and Materials Scientists ; Wiley-VCH: New York, 1993; pp 127-184.

[68] M. R. Gennero De Chivalo, A. C. Chivalo, *Electrochim. Acta,* **1988**, *33,* 825.

[69] R. E. Meyer, *J. Electrochem. Soc.,* **1960**, *107,* 847.

[70] I. Saeki, Y. Sugiyama, S. Hayashi, A. Yamauchi, T. Doi, Y. Nishiyama, S. Kyo, S. Suzuki, M. Sato, S. Fujimoto. *Corrosion Sci.,* **2012**, *55,* 219.

[71] A. P. Grosvenor, B. A. Kobe, M. C. Biesinger, N. S. McIntrye, *Surf. Interface Anal.,* **2004**, *36,* 1564.

[72] M. C. Biesinger, B. P. Payne, A. P. Grosvenor, L. W. M. Lau, A. R. Gerson, R. St. C. Smart, *Appl. Surf. Sci.,* **2011**, *257,* 2717.

[73] C. Klewe, M. Meinert, A. Boehnke, K. Kuepper, E. Arenholz, A. Gupta, J. M. Schmalhorst, T. Kuschel, G. Reiss, *J. Appl. Phys.,* **2014**, *115* (123903), 1−7.

[74] M. Nagayama, M. Kawamura, *Electrochim. Acta,* **1967**, *12,* 1109.

[75] M. E. G. Lyons, M. P. Brandon, *Phys. Chem. Chem. Phys.*, **2009**, *11***,** 2203.

[76] A. Ramirez, P. Hildebrand, D. Stellmach, M. M. May, P. Bogdanoff, S. Fiechter, *J. Phys. Chem. C.,* **2014**, *118,* 14073.

[77] L. R. Czarnetzki, L. J. J. Janssen, *J. Appl. Electrochem.,* **1992**, *22,* 315.

[78] S. Rebouillat, M. E. G. Lyons, M. P. Brandon, R. L. Doyle, *Int. J. Electrochem. Sci.,* **2011**, *6,* 5830.